

Article

The Influencing Mechanisms of Sodium Hexametaphosphate on Chalcopyrite Flotation in the Presence of $MgCl_2$ and $CaCl_2$

Wanqing Li ¹, Yubiao Li ^{1,2,*} , Qing Xiao ², Zhenlun Wei ¹ and Shaoxian Song ¹

¹ School of Resources and Environmental Engineering, Wuhan University of Technology, Wuhan 430070, Hubei, China; wanqing280@163.com (W.L.); erebus@whut.edu.cn (Z.W.); sxx851215@whut.edu.cn (S.S.)

² School of Natural and Built Environments, University of South Australia, Mawson Lakes, SA 5095, Australia; qing.xiao@mymail.unisa.edu.au

* Correspondence: Yubiao.Li@whut.edu.cn

Received: 26 March 2018; Accepted: 8 April 2018; Published: 11 April 2018



Abstract: Sea water has been used in flotation plants, showing a promising way to save fresh water usage. Previous studies indicated that divalent salts in sea water played negative roles in chalcopyrite flotation, but not much work have been conducted to understand the eliminating mechanisms. This study systematically investigated the effects of divalent cations of Ca^{2+} and Mg^{2+} on natural flotability of chalcopyrite in the absence of collectors and frothers. The reduced recovery was mainly due to the adsorption of Mg and Ca hydroxyl complexes and precipitation on chalcopyrite surfaces, giving rise to a less hydrophobic surface. The addition of sodium hexametaphosphate (SHMP), however, significantly improved chalcopyrite recovery. Species calculation, contact angle, zeta potential, FTIR and XPS analyses were conducted to understand the influencing mechanisms of divalent ions and the beneficial effects of SHMP on chalcopyrite recovery. The primary mechanism was that SHMP prevented the adsorption of positively charged Mg and Ca compounds or precipitation with hydrophilic properties such as $Mg(OH)_2$ on chalcopyrite surfaces, confirmed by the Derjugin-Landau-Verwey-Overbeek (DLVO) theory. Secondly, SHMP reacted with Mg^{2+} and Ca^{2+} to form dissolvable complexes, thereby declining the formation of insoluble Mg^{2+} and Ca^{2+} compounds or precipitation.

Keywords: chalcopyrite; flotation; calcium; magnesium; sodium hexametaphosphate

1. Introduction

Mineral flotation, as a water-intensive process, has been widely used to separate valuable minerals from gangue by utilizing differences in physicochemical surface properties [1,2]. Fresh water is normally the most ideal flotation media and the water quality affects flotation efficiency considerably [3]. Due to the continuous growing population and industrial development, the overall water quality is gradually decreasing around the world, resulting in a scarcity of high quality fresh water [4,5]. In order to minimize fresh water consumption and meet the stringent environmental regulations, many concentrators, especially those sited in fresh water-deficient areas, have applied sea water or recycled water with a high concentration of electrolytes, as an alternative to fresh water in flotation process [2,6]. Some typical flotation practices using saline or sea water are summarized in Table 1.

Table 1. Typical flotation practices using saline or sea water.

Concentrator	Location	Processing Content	References
Batu Hijau	Indonesia	Using sea water to process a gold-rich porphyry copper ore	[7]
Las luses	Chile	Grinding and flotation using mixed sea water and tailing dam water	[6]
Çayeli Bakır Is letmeleri A.S.	Turkey	Processing Cu–Zn sulfide ore using dissolved metal ions and sulfide ions (SO_4^{2-} and $\text{S}_2\text{O}_3^{2-}$)	[8]
Mt Keith	Australia	Processing nickel minerals using bore water with high ionic strength	[9]
Raglan	Canada	Flotation without frother using saline water with salt levels ranging 20,000–35,000 ppm	[10]

Inevitably, the application of those solutions with a very high salinity brought many challenges for mineral processing. One of the crucial issues is how to maintain the recovery and grade of valuable minerals as well as minimize the dosage of flotation reagents [3]. In the flotation process, the presence of salt ions can increase the complexity of flotation pulp environment by changing pulp water structure, mineral particle properties (e.g., hydration and electrical double layer) and bubble properties (e.g., bubble coalescence and froth stability), which in turn influencing the mineral–bubble attachment and flotation efficiency [2,11–13]. For instance, some monovalent salts (i.e., NaCl and KCl) were found to enhance mineral flotability by compressing electrical double layers, reducing the energy bar for particle–bubble attachment and even changing bubble stability [14–16]. In contrast, the presence of some divalent cations such as Ca^{2+} and Mg^{2+} might form metal hydroxyl-complexes and colloidal precipitation onto hydrophobic mineral surfaces under alkaline conditions, reducing mineral surface hydrophobicity and the adsorption of collectors [17–19].

As chalcopyrite is the most important Cu-bearing sulfide mineral [20], some attentions have been paid to investigate the effects of saline water on its flotation efficiency. For instance, Haga et al. [21] reported that the Cu grade was improved when conditioning Cu minerals (in which the main valuable mineral is chalcopyrite) into sea water. In a Cu–Au ore flotation with chalcopyrite as the major valuable Cu mineral in the presence of bentonite, Wang et al. [22] found that divalent cations of Mg^{2+} and Ca^{2+} had a more significant role than monovalent cations of Na^+ and K^+ in reducing bentonite viscosity due to stronger compression of electrical double layers of bentonite particles, thereby increasing flotation efficiency, similar to that found in Hirajima et al. [17]. Recently, Li et al. [16] reported that at pH 10, the presence of Na^+ , K^+ , Ca^{2+} increased chalcopyrite recovery due to lower energy barrier for bubble–particle attachments through compressing electrostatic double-layer while the addition of Mg^{2+} decreased chalcopyrite flotation efficiency due to the adsorption of formed $\text{Mg}(\text{OH})_2$ precipitation onto chalcopyrite surface to reduce its hydrophobicity. Although these studies focused on the effects of salts on chalcopyrite flotability through investigating the change of particle surface properties, the flotation results varied and even conflicted, keeping underlying mechanisms unclear.

Many researchers have attempted to relieve or even eliminate the negative effects due to sea water in the mineral flotation process. For instance, Nagaraj and Farinato [23] reported that reducing pH to a lower value can avoid the formation of precipitation, thereby increasing chalcopyrite flotation. However, the alkaline condition at pH 9–12 was used to depress pyrite that normally associated with chalcopyrite [24]. Therefore, it is impractical to reduce the pulp pH to neutral or acidity when using sea water in chalcopyrite flotation. Other researchers have attempted to add some reagents to achieve the goal [19,24–27]. For instance, Jeldres et al. [24] reported that the addition of $\text{CaO-Na}_2\text{CO}_3$ mixtures can remove cations before flotation. Hirajima et al. [17] and Suyantara et al. [28] found that emulsified kerosene was capable of reducing the adsorption of $\text{Mg}(\text{OH})_2$ precipitation on chalcopyrite surface through forming kerosene and precipitation aggregates.

Sodium hexametaphosphate (SHMP, $(\text{NaPO}_3)_6$), normally regarded as a common dispersant, was typically a polymeric metaphosphate in solution [29,30]. In the flotation process, it was widely used to disperse slime that might attach on valuable mineral surfaces, through increasing the repulsive energy between particles [31–34]. For instance, montmorillonite, one fine clay mineral, can inhibit coal flotation due to its adsorption on coal surfaces, decreasing interaction between collectors and coal particles. The addition of SHMP increased the absolute value of zeta potentials of both coal and montmorillonite to enhance electrostatic repulsion, thereby decreasing the adsorption of montmorillonite on coal surfaces [30,35].

In addition, some recently published papers [36,37] have indicated that SHMP can act as a water softener to eliminate the adverse effects of hydrolytic metallic ions in the flotation process. Moreover, Rebolledo et al. [26] reported that the addition of SHMP can remove Mg hydroxyl-complexes and hydroxide from molybdenite surface. However, it is not fully understood that if SHMP has similar positive effects on enhancing chalcopyrite recovery in the presence of divalent cations.

Therefore, a systematic study is necessary to better understand the effects of SHMP on chalcopyrite flotation in the solution containing divalent cations of Ca^{2+} and Mg^{2+} that normally playing a negative role on chalcopyrite flotation. As chalcopyrite is naturally floatable, the flotation experiment was conducted in the absence of collectors and frothers to avoid the influence from those flotation reagents. Various measurements such as contact angle, zeta potential, FTIR, and XPS were carried out to reveal the mechanisms that SHMP imparted on chalcopyrite flotation.

2. Materials and Methods

2.1. Samples and Reagents

A pure chalcopyrite sample was obtained from Australia GEO discoveries. The chalcopyrite chunks were firstly crushed and then ground in a three head grinding machine (RK/XPM, Wuhan Rock Grinding Equipment Manufacturing Co., Ltd, Wuhan, China), followed by a wet sieve and ultrasonic operation to remove fine particles in ethanol solution. Before storing in a freezer to minimize oxidation, the powders were dried in a vacuum oven and sealed in plastic tubes. The particles ranging from 38 to 74 μm were used for flotation tests, while the particles with a size $<38 \mu\text{m}$ were further ground to $-5 \mu\text{m}$ for zeta potential measurements. The XRD spectra (Figure 1) indicated a high purity of chalcopyrite.

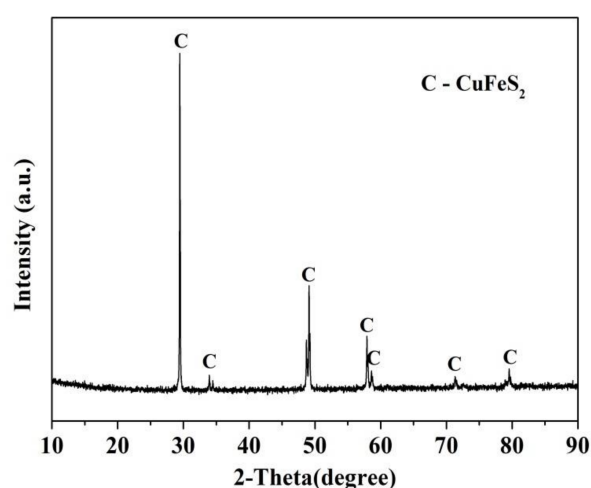


Figure 1. X-ray Diffraction patterns of chalcopyrite.

Analytical grade of reagents including SHMP, sodium hydroxide (NaOH), anhydrous calcium chloride (CaCl_2) and magnesium chloride hexahydrate ($\text{MgCl}_2 \cdot 6\text{H}_2\text{O}$) were purchased from China Sinaopharm Chemical Reagent Co., Ltd, Shanghai, China. In addition, all aqueous solutions were prepared using Millipore® ultrapure water (Billerica, MA, USA) with a resistivity of 18.2 $\text{M}\Omega \cdot \text{cm}$ unless otherwise specified.

2.2. Flotation Experiments

A mechanical agitation XFGII-type flotation machine (Wuhan Exploration Machinery Factory, Wuhan, China) was used for flotation experiments. 1 g of chalcopyrite particle was placed into 25 mL of solution. After that, NaOH was added to maintain the pulp pH to the desired values within the first 6 mins prior to flotation. The collection of concentrate was conducted in the next 5 min of flotation with an air flow rate of 0.1 L/min at an agitation of 1200 rpm. Both the floated and unfloat fractions were collected and air dried at 70 °C for 2 h prior to weighing. It should be noted that 0.01 M CaCl₂ and 0.05 M MgCl₂ were selected for flotation as which were close to that in sea water [2,15]. As the flotation reagents affected chalcopyrite flotability significantly, no reagents were added to investigate the effects of SHMP on the natural flotability in the presence of divalent cations in this study.

2.3. Contact Angle Measurements

The polished chalcopyrite slab was soaked in conditioned solution for 10 mins, followed by rinsing three times using ultrapure water and then air dried. Subsequently, a droplet of ultrapure water (0.25 µL) was placed onto the prepared chalcopyrite slab surface through micro-syringe, thereafter the profile of contact angle was imaged and measured by a sessile drop device (JC2000C1, Shanghai Zhongchen Digital Technology Company, Shanghai, China), with the operating procedures being the same to our previous studies [16]. At least three different areas were selected on each chalcopyrite slab surface and the average value was reported herein.

2.4. Ion Concentration Analyses

In order to investigate the evolution of Ca²⁺ and Mg²⁺ during the flotation process, an inductively coupled plasma (ICP, Optima 4300DV, Perkin, Perkin Elmer Ltd., Waltham, MA, USA) was used to measure the ion concentration before and after flotation.

2.5. Zeta Potential Measurements

A Nano-ZS90 zeta potential analyzer (Malvern Co., Ltd, Malvern, UK) was used to determine the zeta potential of chalcopyrite in different aqueous solutions. Suspensions containing 0.05 g of finely ground samples below −5 µm were conditioned by a magnetic stirrer for 10 min so that the suspension was homogenized. During this period, the pulp pH was adjusted using NaOH solution. After that, the agitated suspension was sampled for zeta potential measurements. Temperature was maintained at 25 ± 1 °C throughout the measurements. The results presented herein were the average of at least three independent tests with a typical variation of ±5 mV.

2.6. FTIR Spectra

A total of 100 mg chalcopyrite particles (−5 µm) were added into 50 mL solution (pH 9.5) with 10 mg/L SHMP. After stirring pulp for 30 min, chalcopyrite particles were filtered and washed thrice using ultrapure water, dried in a vacuum oven over 24 h at room temperature. The dried sample was then mixed with KBr at a mass ratio of 1:100, prior to pressing as thin pellets. The Fourier transform infrared (FTIR) spectra were performed to characterize chalcopyrite surface treated in conditioned solutions at a 4 cm^{−1} resolution within 4000~400 cm^{−1} using Nicolet IS-10 (Thermo Fisher Scientific Inc., Waltham, MA, USA).

2.7. XPS Measurements

The XPS spectra of untreated and treated chalcopyrite particles were determined by ESCALAB 250Xi (Thermo Fisher Scientific Inc., Waltham, MA, USA) equipped with an Al K α monochromatic X-ray source. The survey (wide) spectra were collected from 1350 to 0 eV with a pass energy of 100 eV and a step size of 1.0 eV while the high resolution XPS spectra collected for each element were with a pass energy of 30 eV and a step size of 0.1 eV. The dwell time for both survey and high resolution

spectra was 0.1 s while each spectrum was with 5 sweeps. The C 1s peak at 284.8 eV was used as an internal standard to calibrate all the spectra for charge compensation. All XPS spectra were fitted through XPS Peak4.1 software using Shirley methods for backgrounds corrections [38]. More details regarding the analysis can be referred to that shown in Li et al. [16].

3. Results and discussion

3.1. Flotation Results

Figure 2 shows chalcopyrite recovery as a function of pH from 4 to 12. With the increase of pH, chalcopyrite recoveries were decreased to various extents. For instance, a relatively stable chalcopyrite recovery remaining at approximately 88% was observed in ultrapure water up to pH 9.5, after which recovery was decreased apparently. But more significant declines with increased pH values were found in the presence of CaCl_2 and MgCl_2 , e.g., only around 60% and 28% chalcopyrite were recovered at pH 9.5, respectively, suggesting a negative role due to these two salts, with MgCl_2 being more significant than that of CaCl_2 . In addition, when pH was controlled at 12, only 1% of chalcopyrite was recovered in the MgCl_2 solution.

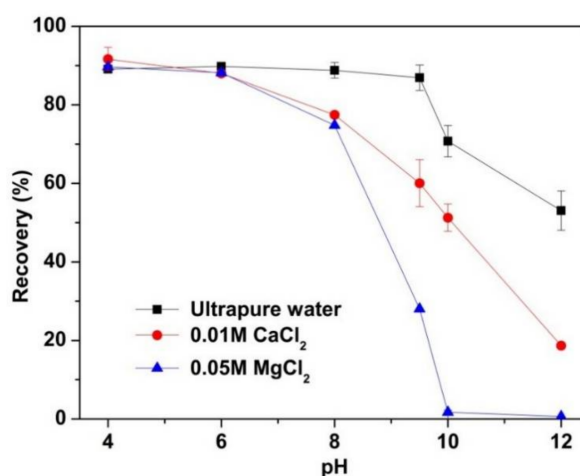


Figure 2. Chalcopyrite recovery as a function of pH.

A similar deteriorative chalcopyrite recovery in ultrapure water controlled at strong alkaline condition was found by Liu and Zhang [39] while detrimental effects of both salts on chalcopyrite recovery were reported in [17,28]. Nagaraj and Farinato [23] reported that Ca^{2+} had a negligible effect while Li et al. [16] reported a slightly beneficial effect on chalcopyrite flotation in the solution containing Ca^{2+} . The differing flotation behaviors of chalcopyrite in salt solution may be attributed to various collectors (e.g., sodium diisobutyl dithiophosphate vs. sodium butyl xanthate) and pulp densities (35 wt % vs. 8 wt %) [40].

Figure 3 shows chalcopyrite recovery as a function of SHMP dosage from 0 to 10 mg/L at pH 9.5. In the absence of Ca^{2+} or Mg^{2+} (i.e., ultrapure water), chalcopyrite recovery was remained at a stable level within 10 mg/L SHMP, suggesting an insignificant role of SHMP in influencing chalcopyrite recovery. However, a gradual increase of chalcopyrite recovery was observed in 0.01 M CaCl_2 solution when SHMP dosage was increased to 10 mg/L. Much greater positive influence of SHMP on chalcopyrite recovery was observed in 0.05 M MgCl_2 solution, e.g., from 28% to approximately 80%. These indicated that the presence of SHMP improved chalcopyrite recovery by depressing the negative role due to CaCl_2 and MgCl_2 .

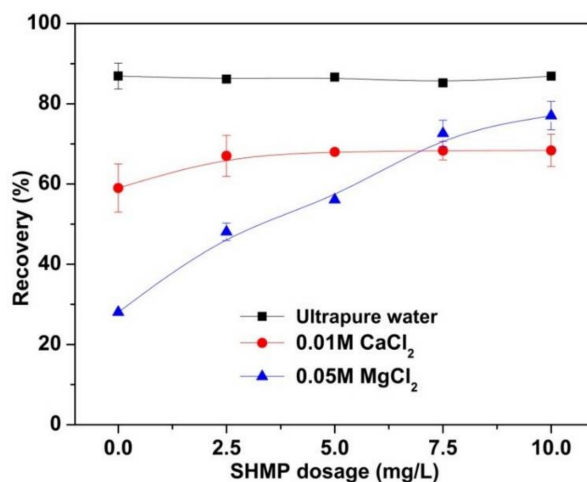


Figure 3. Effects of SHMP dosage on chalcopyrite recovery at pH 9.5.

3.2. Species Calculation

Ca^{2+} and Mg^{2+} ions are typical inevitable metallic ions in sea water. However, complexation and precipitation occurred when solution pH was adjusted to alkaline conditions. Figure 4 shows the formation of calcium hydroxide ($\text{Ca}(\text{OH})_{2(s)}$) and magnesium hydroxide precipitation ($\text{Mg}(\text{OH})_{2(s)}$) at pH greater than 12.4 and 9.3 in 0.01 M CaCl_2 and 0.05 M MgCl_2 solution, respectively. Specifically, Figure 4a showed that both CaOH^+ and $\text{Ca}(\text{OH})_{2(aq)}$ were increased when solution pH was increased from 4 to 12. However, chalcopyrite recovery was gradually decreased within this pH region, indicating that CaOH^+ and $\text{Ca}(\text{OH})_{2(aq)}$ complexes might play a predominantly negative role on chalcopyrite flotation. Choi et al. [14] and Liu and Zhang [39] reported that hydrolyzed species had a strong affinity to a negatively charged solid surface, i.e., chalcopyrite surface in this study. The adsorption of these hydrolyzed species decreased natural hydrophobicity of chalcopyrite surface, thereby reducing its recovery.

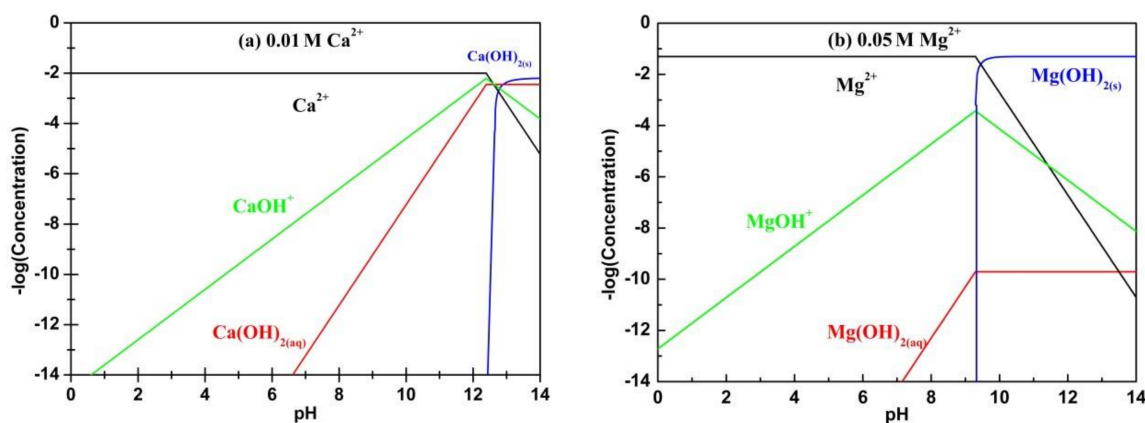
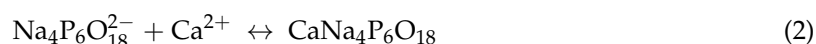
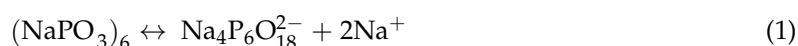


Figure 4. Species of (a) 0.01 M Ca^{2+} and (b) 0.05 M Mg^{2+} .

As indicated in Figure 2, chalcopyrite recovery in 0.05 M MgCl_2 solution was dramatically decreased when pH was increased, achieving a recovery lower than 5% at pH 10 and over. Figure 4b showed three increased Mg^{2+} species including Mg^{2+} , MgOH^+ and $\text{Mg}(\text{OH})_{2(aq)}$ in 0.05 M MgCl_2 solution, within pH from 4 to 9.3. Further increase in pH resulted in Mg precipitation, i.e., $\text{Mg}(\text{OH})_{2(s)}$. Therefore, the decreased chalcopyrite recovery might be due to the adsorption of Mg^{2+} , MgOH^+ and $\text{Mg}(\text{OH})_{2(aq)}$ on negatively charged chalcopyrite surfaces. Specifically, the lowest chalcopyrite

recovery observed at pH 12 was highly likely due to the adsorption of $\text{Mg}(\text{OH})_{2(s)}$ precipitation [23,40]. Therefore, the depressing effects due to divalent cations are normally attributed to the formation of metal complexes and precipitation adsorbed on chalcopyrite surfaces [19,25,39,40].

However, Figure 3 showed that chalcopyrite recovery was increased in both CaCl_2 and MgCl_2 solutions when SHMP was added to flotation pulp controlled at pH 9.5, demonstrating that the presence of SHMP can relieve the negative effects of two salts on chalcopyrite flotation. It should be noted that SHMP can not only act as a dispersant, but also can be used as a complexing agent or softener [26,39] to react with metal cations such as Ca^{2+} and Mg^{2+} , generating soluble complexes (Equations (1)–(3)) [26,34,36,41]. Therefore, the presence of SHMP possibly reduced the formation of Ca and Mg complexes and hydroxide, thereby relieving negative effects of divalent cations.



3.3. Contact Angle Analyses

Figure 5 presents the SHMP effects on contact angle of chalcopyrite conditioned at pH 9.5. In the absence of SHMP, the contact angles of chalcopyrite surface treated in both MgCl_2 and CaCl_2 solution were significantly lower than that in ultrapure water, showing 35° and 56° , respectively, similar to those reported in Li et al. [16] and Hirajima et al. [17]. This suggests that the presence of CaCl_2 and MgCl_2 apparently reduced the chalcopyrite contact angle, possibly due to the adsorption of hydrophilic species formed on the chalcopyrite surface, consistent with the flotation results (Figure 3).

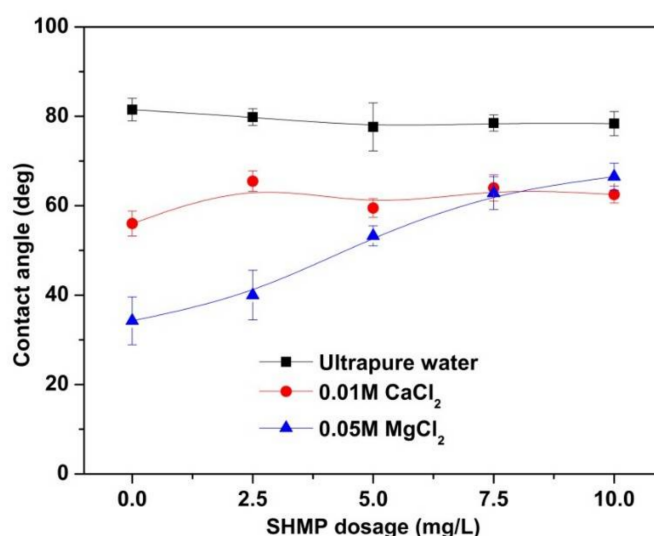


Figure 5. Contact angle of chalcopyrite in the presence of SHMP at pH 9.5.

Although the presence of SHMP did not change the contact angle of chalcopyrite treated in ultrapure water, e.g., almost remaining at 80° , a slight increase was observed in CaCl_2 solutions when SHMP was added, within a relatively narrow range being from 56° to 65° . The above evidence indicated that SHMP reduced the adsorption of Ca complexes on chalcopyrite surfaces in 0.01 M CaCl_2 solution, by reacting with Ca^{2+} to form soluble $\text{CaNa}_4\text{P}_6\text{O}_{18}$ (Equation (2)) [36,37,42]. In contrast, a dramatic increase in contact angle was observed when chalcopyrite was treated in 0.05 M MgCl_2 solution with SHMP dosage being increased up to 10 mg/L, suggesting that SHMP was capable of

removing Mg precipitation or preventing its adsorption on chalcopyrite surface. Therefore, the negative role due to 0.05 M Mg^{2+} was eliminated.

3.4. Zeta Potential Analyses

Figure 6 shows the zeta potentials of chalcopyrite in the presence of SHMP in various solutions controlled at pH 9.5. It is observed that the chalcopyrite surface was negatively charged in ultrapure water, i.e., -43 mV which was increased to positive values of 5 mV and 17 mV in 0.01 M $CaCl_2$ and 0.05 M $MgCl_2$ solution in the absence of SHMP, respectively, probably due to the adsorption of positively charged Ca and Mg species [25,28]. Compared to Ca complexes, $Mg(OH)_{2(s)}$ played a more significant role in reversing chalcopyrite zeta potential to positive values. Choi et al. [14] also reported a similar zeta potential change of malachite from negative to positive when treated in $CaCl_2$ solution. Schott [43] found that the zero point of charge of $Mg(OH)_{2(s)}$ was at pH 10.8, indicating that the zeta potential of $Mg(OH)_{2(s)}$ was positive when pH was lower than 10.8. In other words, $Mg(OH)_{2(s)}$ was positively charged at pH 9.5. Therefore, electrostatic interaction between negatively charged chalcopyrite surface and positively charged Mg precipitation was mainly responsible for chalcopyrite depression by $Mg(OH)_{2(s)}$.

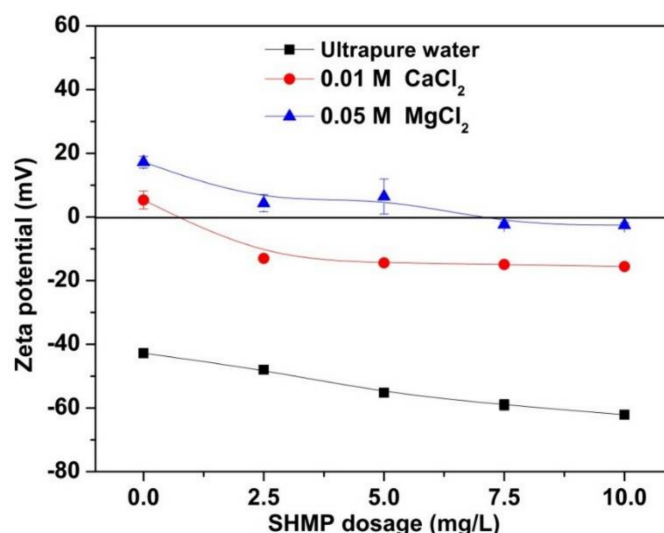


Figure 6. Zeta potential of chalcopyrite in the presence of SHMP at pH 9.5.

When SHMP was added, the zeta potential of chalcopyrite in ultrapure water was more negative with increased SHMP dosage [34]. A significant decrease in zeta potential, i.e., from 5 mV to -15 mV was also observed when 2.5 mg/L SHMP was added into $CaCl_2$ solution. However, no further change in zeta potentials was observed when SHMP dosage was continued to increase. The decrease of zeta potential from a positive value to a negative value might be due to the reduced formation or adsorption of Ca complexes on chalcopyrite surface. Similar to that, in 0.01 M $CaCl_2$ solution, a gradually declined zeta potential was observed in 0.05 M $MgCl_2$ solution when SHMP was added. Although a more positive zeta potential (i.e., 17 mV) was found without SHMP, the reverse to a negative value occurred when SHMP was greater than 7.5 mg/L, indicating that more SHMP was required to reduce negative effects due to $Mg(OH)_{2(s)}$.

In order to further investigate the role of SHMP in the flotation process, the residual concentration of metallic ions in flotation pulp was examined. Figure 7 shows the residual concentration of Ca^{2+} and Mg^{2+} ions in different solutions controlled at pH 9.5. It was found that Ca^{2+} and Mg^{2+} concentrations were 0.01 M and 0.05 M, respectively, prior to flotation, which were decreased to 0.0067 M and 0.038 M,

respectively, after flotation, indicating a loss of these two ions during the flotation process, possibly due to the adsorption or resultant precipitation on chalcopyrite surface.

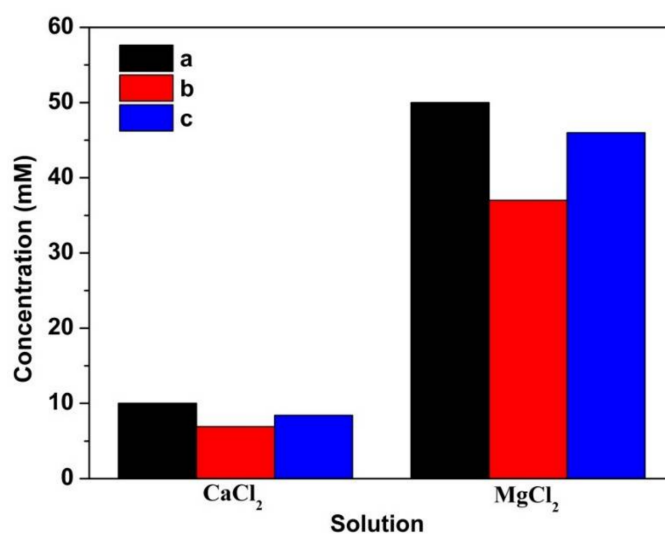


Figure 7. Concentrations of dissolvable Ca and Mg species in the flotation cell, (a) before flotation, (b) after flotation, (c) after flotation with SHMP.

The addition of SHMP reduced cation loss during chalcopyrite flotation. Actually, Ca and Mg concentrations were increased from 0.0067 M to 0.0084 M and 0.038 M to 0.046 M, respectively. It should be noted that the increased Ca and Mg concentrations due to the addition of SHMP were 0.0017 M and 0.008 M, respectively, much greater than the added SHMP (10 mg/L equals to approximately 0.02 mM). According to Equations (1)–(3), the added 0.02 mM SHMP was not capable of combining with so much Ca²⁺ and Mg²⁺. Therefore, in addition to the complexation role, there should be another mechanism for SHMP in enhancing chalcopyrite flotation in CaCl₂ and MgCl₂ solution.

In addition to a complexation role, the dispersion role of SHMP in flotation should be paid more attention as a small amount of SHMP molecules covered in minerals can disperse slime from mineral surfaces [31–34]. Therefore, the dispersion role of SHMP may predominate in enhancing chalcopyrite recovery. In other words, the presence of SHMP prevented Ca or Mg complex adsorption on chalcopyrite surfaces, thereby primarily improving chalcopyrite flotation.

3.5. FTIR Analyses

In order to further verify the role of SHMP on chalcopyrite surface properties, the FTIR spectra of chalcopyrite treated with SHMP were conducted and shown in Figure 8. Figure 8a shows the spectrum of SHMP, where the peaks at 1274.7 and 881.852 cm⁻¹ corresponded to the characteristic adsorption peak of P=O and P–O–P, respectively, while the peaks located at 1093.3 and 1019.3 cm⁻¹ were assigned to P–O stretching vibration [31,34,44,45]. No significant difference was observed in Figure 8b–d, indicating that SHMP was not chemisorbed on chalcopyrite surface [32,45].

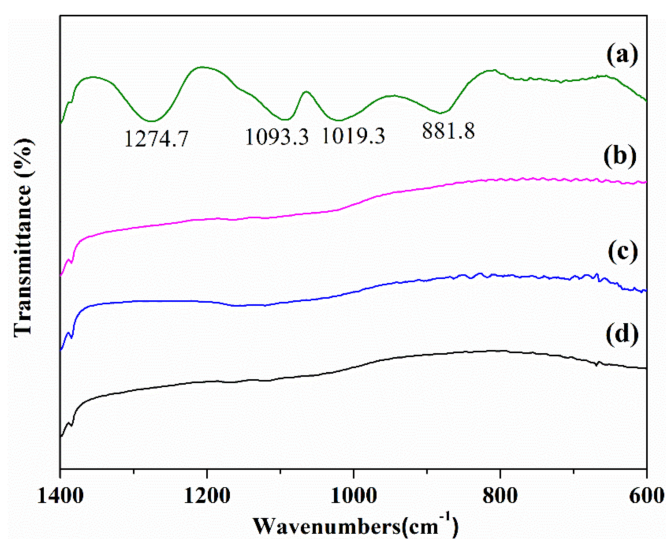


Figure 8. FTIR spectra of (a) SHMP; (b) SHMP + chalcopyrite + $MgCl_2$; (c) SHMP + chalcopyrite + $CaCl_2$; (d) chalcopyrite.

3.6. XPS Analyses

3.6.1. Survey Spectra

XPS analyses were conducted to further investigate the effects of SHMP on Ca and Mg complexes on chalcopyrite surfaces conditioned in different solutions. Figure 9a showed that no Ca was detected on untreated chalcopyrite surfaces. An apparent Ca 2p peak was found when chalcopyrite was treated in 0.01 M $CaCl_2$ solution (Figure 9b), suggesting the adsorption of Ca species on chalcopyrite surface [39]. However, Figure 9c showed that the Ca 2p peak disappeared when 10 mg/L SHMP was added, indicating that SHMP prevented the attachments of Ca species on chalcopyrite.

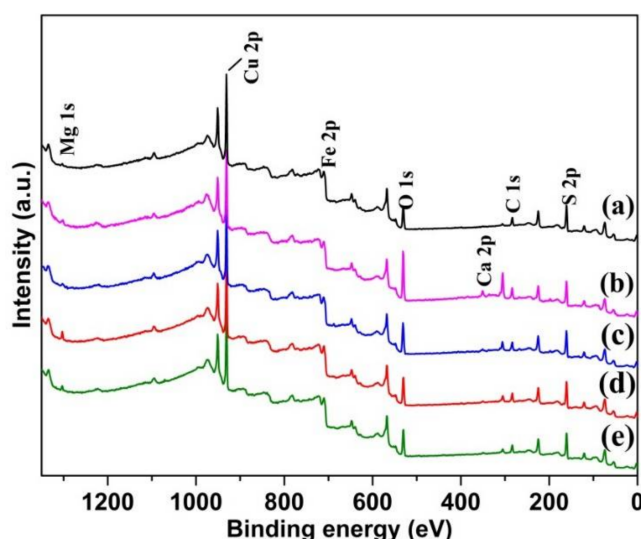


Figure 9. XPS survey spectra of chalcopyrite, (a) untreated, treated in (b) 0.01M $CaCl_2$, (c) 0.01M $CaCl_2$ + SHMP, (d) 0.05 M $MgCl_2$, (e) 0.05 M $MgCl_2$ + SHMP.

Compared to untreated chalcopyrite (Figure 9a), the peak intensity of Mg 1s on a chalcopyrite surface treated in 0.05 M $MgCl_2$ solution (Figure 9d) was increased significantly, indicating the adsorption of Mg precipitation on a chalcopyrite surface. However, the presence of 10 mg/L SHMP

decreased Mg 1s peak intensity (Figure 9e), suggesting that SHMP prevented Mg precipitation on chalcopyrite surface significantly, consistent with contact angle and zeta potential measurements. The detailed atomic percentage of C 1s, S 2p, O 1s, Fe 2p, Cu 2p, Ca 2p and Mg 1s on chalcopyrite surfaces treated under different conditions were shown in Table 2.

Table 2. Elemental quantification (at %) of chalcopyrite surface.

Element	BE (eV)	Conditions				
		Untreated	CaCl ₂	CaCl ₂ + SHMP	MgCl ₂	MgCl ₂ + SHMP
C 1s	284.8	18	20	18	17	18
S 2p	161.5	27	22	26	25	26
O 1s	532.1	19	29	23	23	21
Fe 2p	710.8	16	12	15	15	15
Cu 2p	932.6	19	14	17	17	18
Ca 2p	352.0	0	2	0	0	0
Mg 1s	1304.7	1	1	1	3	2

It is observed that the atomic concentrations of O 1s and Ca 2p on chalcopyrite surfaces were increased after CaCl₂ treatment, confirming the adsorption of Ca complexes on chalcopyrite surfaces. However, the addition of SHMP decreased O 1s and Ca 2p, indicating that SHMP prevented the adsorption of Ca complexes on chalcopyrite, consistent with zeta potential and contact angle measurements.

Similarly, Mg 1s and O 1s were increased from 1 at % to 3 at % and from 19 at % to 23 at %, respectively when the chalcopyrite surface was treated in 0.05 M MgCl₂ solution. The simultaneous and stoichiometric increment in Mg and O highly supported the adsorption of Mg(OH)₂ on chalcopyrite surfaces. In addition, when 10 mg/L SHMP was added, Mg 1s was decreased from 3 at % to 2 at % while O 1s was decreased from 23 at % to 21 at %, further indicating the removal of Mg(OH)₂ from chalcopyrite surface when SHMP was present. In other words, SHMP reduced the formation and adsorption of Mg(OH)₂ on chalcopyrite, thereby improving chalcopyrite recovery.

3.6.2. S 2p Spectra

Figure 10 shows five S species including monosulfide (S²⁻), disulfide (S₂²⁻), polysulfide (S_n²⁻), sulfate (SO₄²⁻) and an energy loss feature (S 3p → Fe 3d) located at 161.3 eV, 162.0 eV, 162.8 eV, 169.1eV and 164.9 eV, respectively [38,46–49].

On the untreated chalcopyrite surface, the concentrations of S²⁻, S₂²⁻, S_n²⁻ and SO₄²⁻ were 58%, 15%, 17% and 5%, respectively (Table 3). The presence of a small portion of SO₄²⁻ indicated that chalcopyrite surface was weakly oxidized by air during grinding or drying process. However, it was reduced to 2 % S and 3 % S when chalcopyrite was treated in 0.01 M CaCl₂ and 0.05 M MgCl₂ solutions, respectively, due possibly to the dissolution of sulfate from chalcopyrite surface into solution [48]. In addition, further decrease was observed when 10 mg/L SHMP was added, indicating that the addition of SHMP was beneficial to SO₄²⁻ dissolution.

Table 3. S species (% S) on chalcopyrite surfaces treated under different conditions.

Species	BE (eV)	FWHM (eV)	Conditions				
			Untreated	CaCl ₂	CaCl ₂ + SHMP	MgCl ₂	MgCl ₂ + SHMP
S ²⁻	161.3	0.7–0.8	58	61	59	62	61
S ₂ ²⁻	162.0	0.7–0.9	15	17	15	14	14
S _n ²⁻	162.8	0.8–1.0	17	15	20	15	17
SO ₄ ²⁻	169.1	1.5–1.6	5	2	0	3	2
Energy loss	164.9	1.4–1.6	5	5	6	6	6

Noted: All BE with a typical variation of ± 0.1 eV.

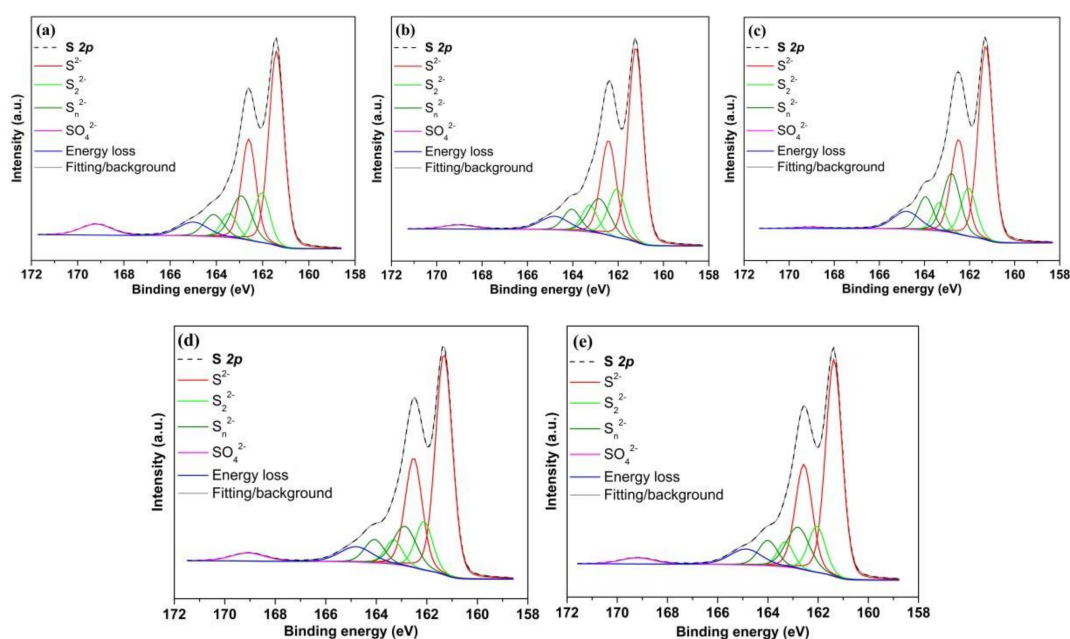


Figure 10. S 2p XPS spectra of (a) untreated chalcopyrite and treated in (b) 0.01 M CaCl₂, (c) 0.01 M CaCl₂ + SHMP, (d) 0.05 M MgCl₂ and (e) 0.05 M MgCl₂ + SHMP.

3.6.3. O 1s Spectra

Figure 11 showed four O species oxide (O²⁻), hydroxide/sulfate (OH⁻/SO₄²⁻), chemisorbed H₂O and physisorbed H₂O located at 530.4, 531.3, 532.1 and 533.5 eV, respectively [38,46,48,50,51]. It should be noted that the hydroxide and sulfate were fitted at 531.3 ± 0.1 eV due to overlapping of the binding energy of these two O species [52]. The presence of oxide on chalcopyrite surface was consistent with the S 2p analysis discussed above.

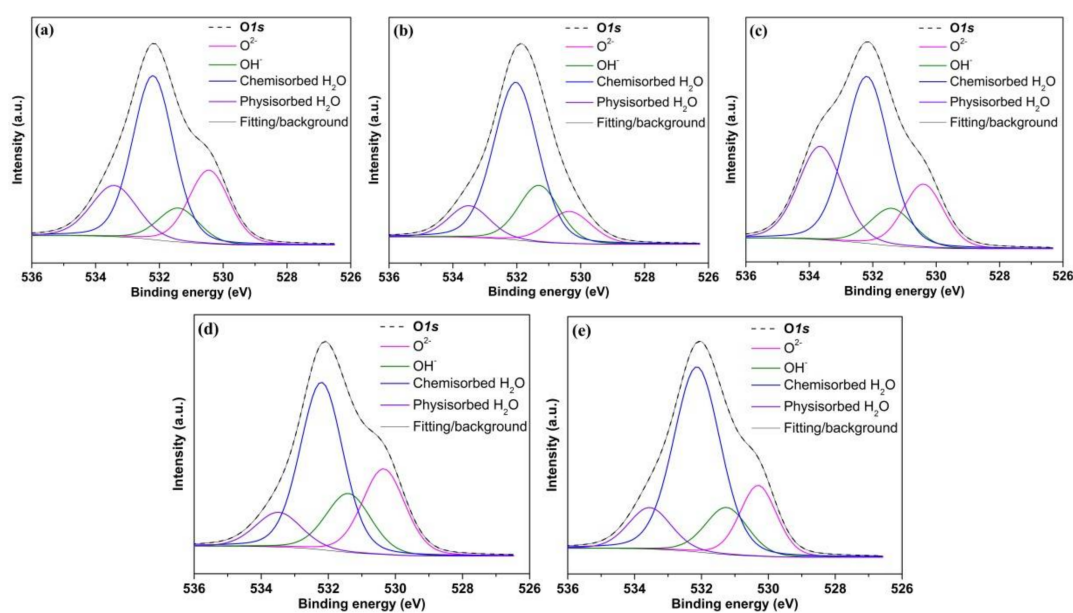


Figure 11. O 1s XPS spectra of (a) untreated chalcopyrite and chalcopyrite treated in (b) 0.01 M CaCl₂, (c) 0.01 M CaCl₂ + 10 mg/L SHMP, (d) 0.05 M MgCl₂ and (e) 0.05 M MgCl₂ + 10 mg/L SHMP.

Table 4 showed that of $\text{OH}^-/\text{SO}_4^{2-}$ concentration was increased from 10 % O to 16 % O and 20 % O when chalcopyrite was treated in CaCl_2 and MgCl_2 solution, respectively. As survey spectra indicated that SO_4^{2-} was decreased when the chalcopyrite surface was treated in a CaCl_2 and MgCl_2 solution (Table 3), the increase of $\text{OH}^-/\text{SO}_4^{2-}$ confirmed the adsorption of more OH^- on chalcopyrite. However, a significant decrease was observed when 10 mg/L SHMP was added, e.g., from 16 % O to 11% O and from 20% O to 13% O, respectively, further suggesting that the addition of SHMP decreased the adsorption of Ca and Mg complexes onto chalcopyrite due primarily to its dispersion effects.

Table 4. O species (% O) on chalcopyrite surfaces treated under different conditions.

Species	BE (eV)	FWHM (eV)	Conditions				
			Untreated	CaCl_2	$\text{CaCl}_2 + \text{SHMP}$	MgCl_2	$\text{MgCl}_2 + \text{SHMP}$
O^{2-}	530.4	1.4–1.5	27	15	18	24	18
$\text{OH}^-/\text{SO}_4^{2-}$	531.3	1.5–1.6	10	16	11	20	13
Chemisorbed H_2O	532.1	1.5–1.7	47	58	47	45	57
Physisorbed H_2O	533.5	1.5–1.7	16	11	24	11	12

3.6.4. Cu 2p Spectra

The Cu $2p_{3/2}$ binding energies across 932.0~932.9 eV, 933.2~933.8 eV and 934.2~936.6 eV were corresponding to Cu in chalcopyrite, Cu oxide and Cu hydroxide, respectively [51,53–56], with the tail at higher binding energy being also possible due to the Cu^{2+} species [57]. As shown in Figure 12, no significant difference in Cu species (detailed values not shown herein) was observed when the chalcopyrite surface was treated under various conditions.

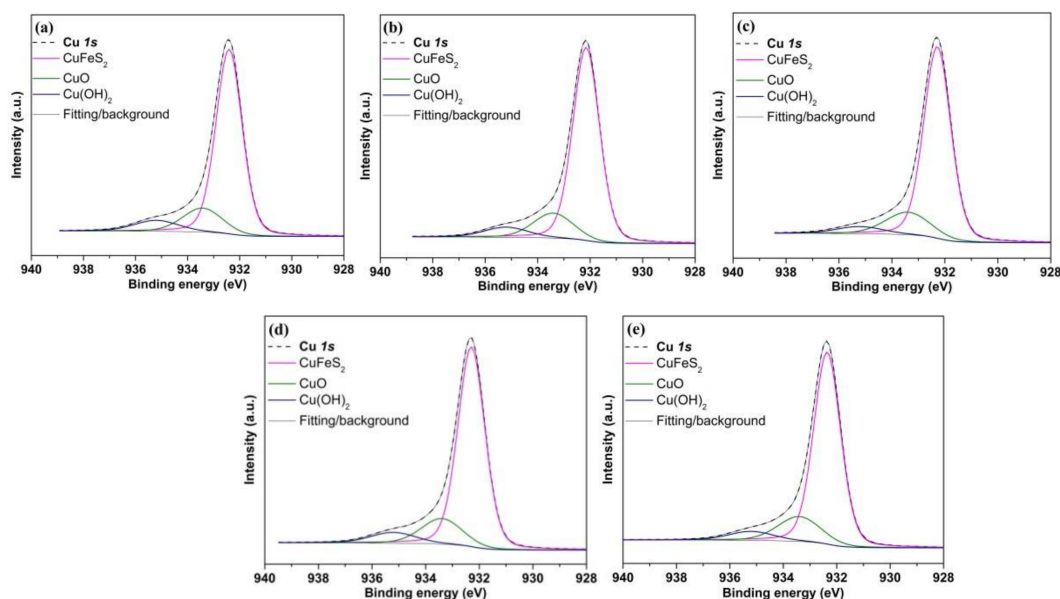


Figure 12. Cu 2p XPS spectrum of (a) untreated chalcopyrite and treated in (b) 0.01 M CaCl_2 , (c) 0.01 M $\text{CaCl}_2 + \text{SHMP}$, (d) 0.05 M MgCl_2 and (e) 0.05 M $\text{MgCl}_2 + \text{SHMP}$.

3.6.5. Fe 2p Spectra

Figure 13 shows the Fe 2p XPS spectra of chalcopyrite treated under different conditions. The strong peaks locating at 708~710 eV and 711~715 eV were assigned to Fe from chalcopyrite and Fe–O/OH/SO species, respectively [46,50,51,58], with the latter being possible from hydrated Fe_2O_3 , $\text{Fe}(\text{OH})_3$, FeOOH and/or $\text{Fe}_2(\text{SO}_4)_3$ formed during the processes of grinding, sieving and flotation, consistent with some other published work [58–60].

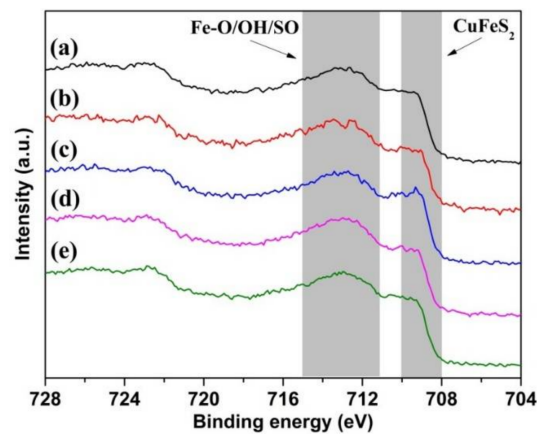


Figure 13. Fe 2p XPS spectra of (a) untreated chalcopyrite and chalcopyrite treated in (b) 0.01 M CaCl₂, (c) 0.01 M CaCl₂ + 10 mg/L SHMP, (d) 0.05 M MgCl₂ and (e) 0.05 M MgCl₂ + 10 mg/L SHMP.

3.7. Mechanisms

The above flotation experiments and measurements indicated that Mg(OH)₂ colloids adversely affected chalcopyrite flotation recovery most significantly, due to its precipitation on chalcopyrite surfaces. Many previous studies demonstrated that the slime coating on the mineral surface was dominated by electrostatic forces [34,35,44,45]. The heterocoagulation phenomenon can be explained by the Derjaguin–Landau–Verwey–Overbeek (DLVO) theory [61,62], in which the total energy V_T between chalcopyrite particles and Mg(OH)₂ colloids equals Van der Waals interaction energy V_W and electrostatic double-layer interaction energy V_E , according to Equation (4) [61,63].

$$V_T = V_W + V_E \quad (4)$$

V_W can be calculated based on Equation (5).

$$V_W = -\frac{A}{6H} \left(\frac{R_1 R_2}{R_1 + R_2} \right) \quad (5)$$

$$A = \left(\sqrt{A_{11}} - \sqrt{A_{33}} \right) \left(\sqrt{A_{22}} - \sqrt{A_{33}} \right) \quad (6)$$

where A refers to the Hamaker constant for chalcopyrite/water/ Mg(OH)₂. The Hamaker constant of chalcopyrite A_{11} is 3.25×10^{-20} J [64]. As Hamaker constant of Mg(OH)₂ cannot be found in literature, the Hamaker constant of MgO ($A_{22} = 10.6 \times 10^{-20}$ J) was applied. The Hamaker constant of water A_{33} is 3.7×10^{-20} J [63,65]. According to particle size analysis, the average diameters (d_{50}) of chalcopyrite particle and Mg(OH)₂ colloids were approximately 70 μm and 7.6 μm , respectively. Therefore, the radius of chalcopyrite particle (R_1) was set as 35 μm while the radius of Mg(OH)₂ colloid (R_2) was 3.8 μm . H (nm) refers to the distance between particles.

The dispersive role of SHMP was achieved through increasing the absolute value of mineral surface potential, further increasing electrostatic repulsive energy between particles. Therefore, V_E between chalcopyrite particles and Mg(OH)₂ colloid was calculated according to Equation (7) [62,63].

$$V_E = \frac{\pi \epsilon_0 \epsilon_r R_1 R_2}{R_1 + R_2} \left(\psi_1^2 + \psi_2^2 \right) \cdot \left\{ \frac{2\psi_1 \psi_2}{\psi_1^2 + \psi_2^2} \cdot \ln \left[\frac{1 + \exp(-\kappa H)}{1 - \exp(-\kappa H)} \right] + \ln[1 - \exp(-2\kappa H)] \right\} \quad (7)$$

where ϵ_0 and ϵ_r represent the vacuum dielectric constant and absolute dielectric constant of the continuous phase, with a given value of 6.95×10^{-10} C²/(J·m) [66]. ψ_1 and ψ_2 (mV) stand for the surface potentials of chalcopyrite and Mg(OH)₂ particles, respectively. In the absence of SHMP,

the surface potentials (zeta potentials) of chalcopyrite and $\text{Mg}(\text{OH})_2$ were 11.2 mV and 15.3 mV, respectively, which were reduced to -21.3 mV and -8.0 mV, respectively in the presence of 10 mg/L SHMP. κ^{-1} is the thickness of electric double-layer, $\kappa = 0.180 \text{ nm}^{-1}$ [34].

Usually, a more negative V_T between particles indicates a more stronger attraction force while a more positive V_T reveals a more stronger repulsive force [61,62]. Figure 14 shows V_T between chalcopyrite and $\text{Mg}(\text{OH})_2$ colloids with and without SHMP. In the absence of SHMP, V_T between chalcopyrite and $\text{Mg}(\text{OH})_2$ colloids was negative within all particle distances examined, indicated that $\text{Mg}(\text{OH})_2$ colloids can be easily attached to chalcopyrite particles, forming aggregation. In contrast, in the presence of SHMP, the V_T between chalcopyrite and $\text{Mg}(\text{OH})_2$ colloids was reversed from negative to positive values, indicating that the attraction force was significantly reduced and the repulsion force was dominated. This is the primary mechanism that SHMP contributed to better chalcopyrite recovery in the presence of Mg^{2+} , e.g., preventing the adsorption of $\text{Mg}(\text{OH})_2$ colloids on chalcopyrite surface.

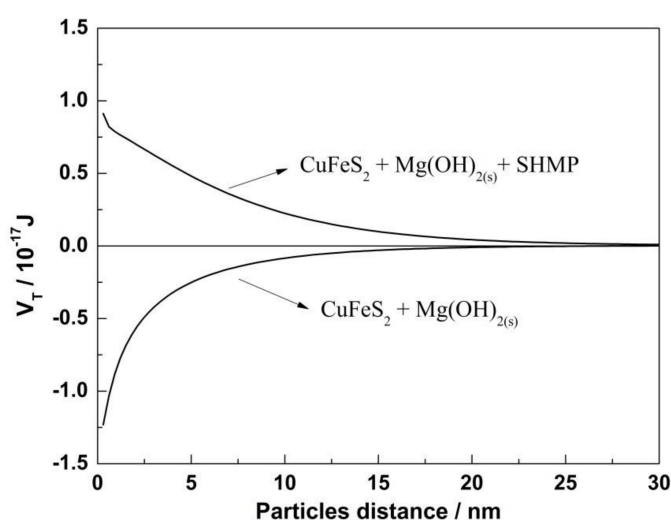


Figure 14. Electrostatic interaction energy between chalcopyrite and magnesium hydroxide colloids.

4. Conclusions

Chalcopyrite recovery was significantly reduced in both 0.01 M CaCl_2 and 0.05 M MgCl_2 solution under alkaline conditions, mainly due to the formation of metallic cations complexes and precipitation onto chalcopyrite surface, giving rise to a less hydrophobic surface. It was found that SHMP played an insignificant role on chalcopyrite recovery in ultrapure water, but apparently relieved the inhibition effects of Ca^{2+} and Mg^{2+} on chalcopyrite flotation. Various measurements indicated that the addition of SHMP decreased zeta potential of chalcopyrite particles and prevented the adsorption of positively charged Ca and Mg species which were hydrophilic, thereby increasing chalcopyrite recovery in the presence of Ca^{2+} and Mg^{2+} under alkaline conditions. This is the primary mechanism that SHMP contributed to better chalcopyrite flotation. In addition, a portion of SHMP reacted with Ca^{2+} and Mg^{2+} to form dissolvable complexes, reducing the formation of precipitation. Further theory calculation indicated that the predominantly beneficial effect of SHMP was assigned to the reverse of interaction force between chalcopyrite and magnesium hydroxide colloids, i.e., from attraction force to repulsion force, thereby preventing the adsorption of hydrophilic magnesium hydroxide on chalcopyrite surface. This study, for the first time, clearly and qualitatively presents two mechanisms of SHMP in improving chalcopyrite recovery in the presence of 0.01 M CaCl_2 and 0.05M MgCl_2 .

Acknowledgments: Financial supports to the project are provided by the National Natural Science Foundation of China (51604205, 51774223) and Natural Science Foundation of Hubei Province (2016CFB268). The authors also thank the supports from Fundamental Research Funds for the Central Universities (WUT: 2016IVA046 and

2017IVB018). A special thank is given to the financial support for the Excellent Dissertation Cultivation Fund of Wuhan University of Technology (2017-YS-052).

Author Contributions: Yubiao Li designed the experiment and wrote the manuscript while Wanqing Li run the experiment and collected all the data. Qing Xiao involved in the discussion of the results and approved reading the manuscript and Shaoxian Song reviewed and edited the manuscript.

Conflicts of Interest: The authors declare no conflict of interest. The founding sponsors had no role in the design of the study; in the collection, analyses, or interpretation of data; in the writing of the manuscript, and in the decision to publish the results.

References

1. Farrokhpay, S. The significance of froth stability in mineral flotation—A review. *Adv. Colloid Interface Sci.* **2011**, *166*, 1–7. [[CrossRef](#)] [[PubMed](#)]
2. Wang, B.; Peng, Y. The effect of saline water on mineral flotation—A critical review. *Miner. Eng.* **2014**, *66–68*, 13–24. [[CrossRef](#)]
3. Liu, W.; Moran, C.; Vink, S. A review of the effect of water quality on flotation. *Miner. Eng.* **2013**, *53*, 91–100. [[CrossRef](#)]
4. Castro, S.; Laskowski, J.S. Froth flotation in saline water. *Kona Powder Part. J.* **2011**, *29*, 4–15. [[CrossRef](#)]
5. Greenlee, L.; Lawler, D.; Freeman, B.; Marrot, B.; Moulin, P. Reverse osmosis desalination: Water sources, technology, and today's challenges. *Water Res.* **2009**, *43*, 2317–2348. [[CrossRef](#)] [[PubMed](#)]
6. Moreno, P.A.; Aral, H.; Cuevas, J.; Monardes, A.; Adaro, M.; Norgate, T.; Bruckard, W. The use of seawater as process water at Las Luces copper–molybdenum beneficiation plant in Taltal (Chile). *Miner. Eng.* **2011**, *24*, 852–858. [[CrossRef](#)]
7. Castro, S. Challenges in flotation of Cu–Mo sulfide ores in sea water. In *The First International Symposium on Water in Mineral Processing*; Drelich, J., Ed.; Society for Mining, Metallurgy, and Exploration: Seattle, WA, USA, 2012.
8. Bıçak, Ö.; Ekmekçi, Z.; Can, M.; Öztürk, Y. The effect of water chemistry on froth stability and surface chemistry of the flotation of a Cu–Zn sulfide ore. *Int. J. Miner. Process.* **2012**, *102*, 32–37. [[CrossRef](#)]
9. Peng, Y.; Seaman, D. The flotation of slime–fine fractions of Mt. Keith pentlandite ore in de-ionised and saline water. *Miner. Eng.* **2011**, *5*, 479–481. [[CrossRef](#)]
10. Quinn, J.J.; Kracht, W.; Gomez, C.O.; Gagnon, C.; Finch, J.A. Comparing the effect of salts and frother (MIBC) on gas dispersion and froth properties. *Miner. Eng.* **2007**, *20*, 1296–1302. [[CrossRef](#)]
11. Cao, Q.; Wang, X.; Miller, J.D.; Cheng, F.; Jiao, Y. Bubble attachment time and FTIR analysis of water structure in the flotation of sylvite, bischofite and carnallite. *Miner. Eng.* **2011**, *24*, 108–114. [[CrossRef](#)]
12. Castro, S.; Miranda, C.; Toledo, P.; Laskowski, J.S. Effect of frothers on bubble coalescence and foaming in electrolyte solutions and seawater. *Int. J. Miner. Process.* **2013**, *124*, 8–14. [[CrossRef](#)]
13. Corin, K.C.; Reddy, A.; Miyen, L.; Wiese, J.G.; Harris, P.J. The effect of ionic strength of plant water on valuable mineral and gangue recovery in a platinum bearing ore from the Merensky reef. *Miner. Eng.* **2011**, *24*, 131–137. [[CrossRef](#)]
14. Choi, J.; Choi, S.Q.; Park, K.; Han, Y.; Kim, H. Flotation behaviour of malachite in mono- and di-valent salt solutions using sodium oleate as a collector. *Int. J. Miner. Process.* **2016**, *146*, 38–45. [[CrossRef](#)]
15. Jeldres, R.I.; Forbes, L.; Cisternas, L.A. Effect of seawater on sulfide ore flotation: A review. *Miner. Process. Extr. Metall. Rev.* **2016**, *37*, 369–384. [[CrossRef](#)]
16. Li, Y.; Li, W.; Xiao, Q.; He, N.; Ren, Z.; Lartey, C.; Gerson, A. The influence of common monovalent and divalent chlorides on chalcopyrite flotation. *Minerals* **2017**, *7*, 111. [[CrossRef](#)]
17. Hirajima, T.; Suyantara, G.P.W.; Ichikawa, O.; Elmahdy, A.M.; Miki, H.; Sasaki, K. Effect of Mg^{2+} and Ca^{2+} as divalent seawater cations on the floatability of molybdenite and chalcopyrite. *Miner. Eng.* **2016**, *96–97*, 83–93. [[CrossRef](#)]
18. Laskowski, J.S.; Castro, S. Hydrolyzing Ions in Flotation Circuits: Sea Water Flotation. In *Proceedings of the 13th International Mineral Processing Symposium, Bodrum, Turkey, 10–12 October 2012*; pp. 219–228.
19. Suyantara, G.P.W.; Hirajima, T.; Elmahdy, A.M.; Miki, H.; Sasaki, K. Effect of kerosene emulsion in $MgCl_2$ solution on the kinetics of bubble interactions with molybdenite and chalcopyrite. *Colloids Surf. A Physicochem. Eng. Asp.* **2016**, *501*, 98–113. [[CrossRef](#)]

20. Li, Y.; Kawashima, N.; Li, J.; Chandra, A.P.; Gerson, A.R. A review of the structure, and fundamental mechanisms and kinetics of the leaching of chalcopyrite. *Adv. Colloid Interface Sci.* **2013**, *197–198*, 1–32. [[CrossRef](#)] [[PubMed](#)]
21. Haga, K.; Nishioka, K.; Altansukh, B.; Shibayama, A. Floatability and bubble behavior in seawater flotation for the recovering copper mineral. *Int. J. Soc. Mater. Eng. Resour.* **2014**, *20*, 82–86. [[CrossRef](#)]
22. Wang, Y.; Peng, Y.; Nicholson, T.; Lauten, R.A. The role of cations in copper flotation in the presence of bentonite. *Miner. Eng.* **2016**, *96–97*, 108–112. [[CrossRef](#)]
23. Nagaraj, D.R.; Farinato, R. Chemical factor effects in saline and hypersaline waters in the flotation of Cu and Cu-Mo ores. In Proceedings of the XXVII International Mineral Processing Congress, Santiago, Chile, 20–24 October 2014.
24. Jeldres, R.I.; Arancibia-Bravo, M.P.; Reyes, A.; Aguirre, C.E.; Cortes, L.; Cisternas, L.A. The impact of seawater with calcium and magnesium removal for the flotation of copper-molybdenum sulphide ores. *Miner. Eng.* **2017**, *109*, 10–13. [[CrossRef](#)]
25. Qiu, Z.; Liu, G.; Liu, Q.; Zhong, H.; Zhang, M. Separation of pyrite from chalcopyrite and molybdenite by using selective collector of *N*-isopropoxypropyl-*N'*-ethoxycarbonyl thiourea in high salinity water. *Miner. Eng.* **2017**, *100*, 93–98. [[CrossRef](#)]
26. Rebolledo, E.; Laskowski, J.S.; Gutierrez, L.; Castro, S. Use of dispersants in flotation of molybdenite in seawater. *Miner. Eng.* **2017**, *100*, 71–74. [[CrossRef](#)]
27. Wan, H.; Yang, W.; He, T.; Yang, J.; Guo, L.; Peng, Y. The influence of Ca²⁺ and pH on the interaction between PAHs and molybdenite edges. *Minerals* **2017**, *7*, 104. [[CrossRef](#)]
28. Suyantara, G.P.W.; Hirajima, T.; Miki, H.; Sasaki, K. Floatability of molybdenite and chalcopyrite in artificial seawater. *Miner. Eng.* **2018**, *115*, 117–130. [[CrossRef](#)]
29. Wang, Y.; Chen, X.; Hu, Y.; Lan, Y. Influences of phosphates on dispersion of fine alumin-silicate minerals. *Cent. South Univ. Sci. Technol.* **2007**, *38*, 238–244.
30. Xu, D.; Zhu, S.; Cao, G.; Cu, H. Influences of sodium hexametaphosphate on dispersion of fine montmorillonite in coal flotation. *J. China Coal Soc.* **2016**, *41*, 192–198.
31. Feng, B.; Wang, P.; Lu, Y.; Feng, Q. Role of sodium hexametaphosphate in flotation of a nickel ore. *Physicochem. Probl. Miner. Process.* **2015**, *51*, 170–181.
32. Feng, Q.; Zhou, Q.; Zhang, G.; Lu, Y.; Yang, S. Inhibition mechanism of sodium hexametaphosphate on calcite. *Chin. J. Nonferr. Met.* **2011**, *21*, 436–441.
33. Long, T.; Feng, Q.; Lu, Y. Dispersive mechanism of sodium hexametaphosphate on flotation of copper-nickel sulphide. *Chin. J. Nonferr. Met.* **2012**, *22*, 1763–1769.
34. Lu, Y.; Zhang, M.; Feng, Q.; Long, T.; Ou, L.; Zhang, G. Effect of sodium hexametaphosphate on separation of serpentine from pyrite. *Trans. Nonferr. Met. Soc. China* **2011**, *21*, 208–213. [[CrossRef](#)]
35. Zhang, M.; Liu, J.; Liu, H.; Wang, Y. Effects of water hardness on the dispersion of fine coal and montmorillonite. *J. China Univ. Min. Technol.* **2009**, *38*, 114–118.
36. Luo, N.; Wei, D.; Shen, Y.; Han, C.; Zhang, C. Elimination of the adverse effect of calcium ion on the flotation separation of magnesite from dolomite. *Minerals* **2017**, *7*, 150. [[CrossRef](#)]
37. Zhang, G.; zhu, Y.; Cui, M. Effect of sodium hexametaphosphate on flotation separation of rhodochrosite from calcite. *Chin. J. Nonferr. Met.* **2012**, *22*, 3214–3220.
38. Ghahremaninezhad, A.; Dixon, D.G.; Asselin, E. Electrochemical and XPS analysis of chalcopyrite (CuFeS₂) dissolution in sulfuric acid solution. *Electrochim. Acta* **2013**, *87*, 97–112. [[CrossRef](#)]
39. Liu, Q.; Zhang, Y. Effect of calcium ions and citric acid on the flotation separation of chalcopyrite from galena using dextrin. *Miner. Eng.* **2000**, *13*, 1405–1416. [[CrossRef](#)]
40. Ramos, O.; Castro, S.; Laskowski, J.S. Copper-molybdenum ores flotation in sea water: Floatability and frothability. *Miner. Eng.* **2013**, *53*, 108–112. [[CrossRef](#)]
41. Ni, X.; Liu, Q. Adsorption behaviour of sodium hexametaphosphate on pyrochlore and calcite. *Can. Metall. Q.* **2013**, *52*, 473–478. [[CrossRef](#)]
42. Ding, H.; Lin, H.; Deng, Y. Depressing effect of sodium hexametaphosphate on apatite in flotation of rutile. *J. Univ. Sci. Technol. Beijing* **2007**, *14*, 200–203. [[CrossRef](#)]
43. Schott, H. Electrokinetic studies of magnesium hydroxide. *J. Pharm. Sci.* **1981**, *70*, 486–489. [[CrossRef](#)] [[PubMed](#)]
44. Li, Z.; Han, Y.; Li, Y.; Gao, P. Effect of serpentine and sodium hexametaphosphate on ascharite flotation. *Trans. Nonferr. Met. Soc. China* **2017**, *27*, 1841–1848. [[CrossRef](#)]

45. Xia, Q.; Li, Z.; Qiu, X.; Dai, Z. Investigation of action mechanism between sodium hexametaphosphate and serpenine. *Min. Metall. Eng.* **2002**, *22*, 53–56.
46. Li, Y.; Chandra, A.P.; Gerson, A.R. Scanning photoelectron microscopy studies of freshly fractured chalcopyrite exposed to O₂ and H₂O. *Geochim. Cosmochim. Acta* **2014**, *133*, 372–386. [[CrossRef](#)]
47. Li, Y.; Qian, G.; Brown, P.L.; Gerson, A.R. Chalcopyrite dissolution: Scanning photoelectron microscopy examination of the evolution of sulfur species with and without added iron or pyrite. *Geochim. Cosmochim. Acta* **2017**, *212*, 33–47. [[CrossRef](#)]
48. Li, Y.; Qian, G.; Li, J.; Gerson, A.R. Kinetics and roles of solution and surface species of chalcopyrite dissolution at 650 mV. *Geochim. Cosmochim. Acta* **2015**, *161*, 188–202. [[CrossRef](#)]
49. Vizcarra, T.G.; Harmer, S.L.; Wightman, E.M.; Johnson, N.W.; Manlapig, E.V. The influence of particle shape properties and associated surface chemistry on the flotation kinetics of chalcopyrite. *Miner. Eng.* **2011**, *24*, 807–816. [[CrossRef](#)]
50. Acres, R.G.; Harmer, S.L.; Beattie, D.A. Synchrotron XPS, NEXAFS, and ToF-SIMS studies of solution exposed chalcopyrite and heterogeneous chalcopyrite with pyrite. *Miner. Eng.* **2010**, *23*, 928–936. [[CrossRef](#)]
51. Yin, Z.; Sun, W.; Hu, Y.; Zhang, C.; Guan, Q.; Liu, R.; Chen, P.; Tian, M. Utilization of acetic acid-[(hydrazinylthioxomethyl)thio]-sodium as a novel selective depressant for chalcopyrite in the flotation separation of molybdenite. *Sep. Purif. Technol.* **2017**, *179*, 248–256. [[CrossRef](#)]
52. Nesbitt, H.W.; Muir, I.J. Oxidation states and speciation of secondary products on pyrite and arsenopyrite reacted with mine waste waters and air. *Mineral. Petrol.* **1998**, *62*, 123–144. [[CrossRef](#)]
53. Fujisawa, M.; Suga, S.; Mizokawa, T.; Fujimori, A.; Sato, K. Electronic structures of CuFeS₂ and CuAl_{0.9}Fe_{0.1}S₂ studied by electron and optical spectroscopies. *Phys. Rev. B* **1994**, *49*, 7155–7164. [[CrossRef](#)]
54. Guo, Y.; Cui, K.; Hu, M.; Jin, S. Fe(III) ions enhanced catalytic properties of (BiO)₂CO₃ nanowires and mechanism study for complete degradation of xanthate. *Chemosphere* **2017**, *181*, 190–196. [[CrossRef](#)] [[PubMed](#)]
55. Harmer, S.L.; Thomas, J.E.; Fornasiero, D.; Gerson, A.R. The evolution of surface layers formed during chalcopyrite leaching. *Geochim. Cosmochim. Acta* **2006**, *70*, 4392–4402. [[CrossRef](#)]
56. Wang, J.; Xie, L.; Liu, Q.; Zeng, H. Effects of salinity on xanthate adsorption on sphalerite and bubble–sphalerite interactions. *Miner. Eng.* **2015**, *77*, 34–41. [[CrossRef](#)]
57. Buckley, A.N.; Skinner, W.M.; Harmer, S.L.; Pring, A.; Lamb, R.N.; Fan, L.J.; Yang, Y.W. Examination of the proposition that Cu(II) can be required for charge neutrality in a sulfide lattice—Cu in tetrahedrites and sphalerite. *Can. J. Chem.* **2007**, *85*, 767–781. [[CrossRef](#)]
58. Hirajima, T.; Miki, H.; Suyantara, G.P.W.; Matsuoka, H.; Elmahdy, A.M.; Sasaki, K.; Imaizumi, Y.; Kuroiwa, S. Selective flotation of chalcopyrite and molybdenite with H₂O₂ oxidation. *Miner. Eng.* **2017**, *100*, 83–92. [[CrossRef](#)]
59. Kalegowda, Y.; Chan, Y.; Wei, D.; Harmer, S.L. X-PEEM, XPS and ToF-SIMS characterisation of xanthate induced chalcopyrite flotation: Effect of pulp potential. *Surf. Sci.* **2015**, *635*, 70–77. [[CrossRef](#)]
60. Owusu, C.; Fornasiero, D.; Addai-Mensah, J.; Zanin, M. Influence of pulp aeration on the flotation of chalcopyrite with xanthate in chalcopyrite/pyrite mixtures. *Int. J. Miner. Process.* **2015**, *134*, 50–57. [[CrossRef](#)]
61. Adamczyk, Z.; Weroński, P. Application of the DLVO theory for particle deposition problems. *Adv. Colloid Interface Sci.* **1999**, *83*, 137–226. [[CrossRef](#)]
62. Missana, T.; Adell, A. On the applicability of DLVO theory to the prediction of clay colloids stability. *J. Colloid Interface Sci.* **2000**, *230*, 150–156. [[CrossRef](#)] [[PubMed](#)]
63. Ren, J.; Shen, J.; Luo, S. *Particle Dispersion Science and Technology*; Chemical Industry Publisher: Beijing, China, 2005.
64. Sharma, P.K.; Rao, K.H. Adhesion of paenibacillus polymyxa on chalcopyrite and pyrite: Surface thermodynamics and extended DLVO theory. *Colloids Surf. B Biointerfaces* **2003**, *29*, 21–38. [[CrossRef](#)]
65. Van Oss, C.J.; Giese, R.F.; Costanzo, P.M. DLVO and non-DLVO interactions in hectorite. *Clays Clay Miner.* **1990**, *38*, 151–159. [[CrossRef](#)]
66. Feng, B.; Lu, Y.; Feng, Q.; Li, H. Solution chemistry of sodium silicate and implications for pyrite flotation. *Ind. Eng. Chem. Res.* **2012**, *51*, 12089–12094. [[CrossRef](#)]

